

# Diffuse scattering from the lead-based relaxor ferroelectric $\text{PbMg}_{1/3}\text{Ta}_{2/3}\text{O}_3$

A. Cervellino,<sup>1,2</sup> S.N. Gvasaliya,<sup>2</sup> O. Zaharko,<sup>2</sup> B. Roessli,<sup>2</sup> G.M. Rotaru,<sup>2</sup>  
R.A. Cowley,<sup>3</sup> S.G. Lushnikov,<sup>4</sup> T.A. Shaplygina,<sup>4</sup> and M.-T. Fernandez-Diaz<sup>5</sup>

<sup>1</sup>*Swiss Light Source, Paul Scherrer Institute, CH-5232 Villigen, Switzerland*

<sup>2</sup>*Laboratory for Neutron Scattering,*

*ETHZ & PSI, CH-5232 Villigen, Switzerland*

<sup>3</sup>*Clarendon Laboratory, Department of Physics,*

*Oxford University Parks Road, Oxford, OX1 3PU, UK*

<sup>4</sup>*Ioffe Physical Technical Institute, 194021 St. Petersburg, Russia*

<sup>5</sup>*Institut Laue-Langevin, 156X, 38042 Grenoble Cédex, France*

(Dated: November 26, 2021)

## Abstract

The relaxor ferroelectric  $\text{PbMg}_{1/3}\text{Ta}_{2/3}\text{O}_3$  was studied by single-crystal neutron and synchrotron x-ray diffraction and its detailed atomic structure has been modeled in terms of static Pb-displacements that lead to the formation of polar nanoregions. Similar to the other members of the Pb-based relaxor family like  $\text{PbMg}_{1/3}\text{Nb}_{2/3}\text{O}_3$  or  $\text{PbZn}_{1/3}\text{Nb}_{2/3}\text{O}_3$  the diffuse scattering in the  $[\text{H},0,0]/[0,\text{K},0]$  scattering plane has a butterfly-shape around the  $(\text{h},0,0)$  Bragg reflections and is transverse to the scattering vector for  $(\text{h},\text{h},0)$  peaks. In the  $[\text{H},\text{H},0]/[0,0,\text{L}]$  plane the diffuse scattering is elongated along the  $\langle 1,1,2 \rangle$  directions and is transverse to the scattering vector for  $(\text{h},\text{h},\text{h})$  reflections. We find that a model consisting of correlated Pb-displacements along the  $\langle 1,1,1 \rangle$ -directions reproduces the main features of the diffuse scattering in  $\text{PbMg}_{1/3}\text{Ta}_{2/3}\text{O}_3$  adequately when the correlation lengths between the Pb-ion displacement vectors are longest along the  $\langle 1,1,1 \rangle$  and  $\langle 1,-1,0 \rangle$  and shortest along  $\langle 1,1,-2 \rangle$  directions.

PACS numbers: 77.80.-e Ferroelectricity and antiferroelectricity; 77.84.-s Dielectric, piezoelectric, ferroelectric, and antiferroelectric materials; 61.05.C X-ray diffraction and scattering; 61.43.Bn Structural modeling: serial-addition models, computer simulation;

## I. INTRODUCTION

Cubic perovskites  $AB'_x B''_{1-x} O_3$  with random occupation of the B site form a special class of ferroelectrics. In these materials the dielectric permittivity has a maximum around  $T_{\max}$  that is not associated with any structural phase transition. Because the maximum of the dielectric constant is broad in temperature and also depends on the frequency, these materials are called "relaxor ferroelectrics".  $PbB'_{1/3} B''_{2/3} O_3$  ( $B' = \text{Zn, Mg}$ ;  $B' = \text{Nb, Ta}$ ) are typical relaxor ferroelectrics. To explain the broad maximum in the dielectric permittivity it was proposed by Smolenskii [1] that fluctuations in  $B' : B''$  ions lead to a coexistence of polar and non-polar regions in these materials as the temperature is reduced. Later Burns [2] used the same approach to explain the temperature dependence of the refraction index that polar regions of nanometer size (PNR) form below a characteristic temperature, which for  $PbMg_{1/3} Nb_{2/3} O_3$  (PMN) is  $T_d \sim 620$  K.

Extensive studies of the phonons in relaxor ferroelectrics by inelastic neutron scattering were unable to identify the soft mode that together with the Lyddane-Sachs-Teller relationship would explain the temperature dependence of the dielectric permittivity. Recently, however, it was shown that a quasi-elastic mode appears below the Burns temperature in PMN whose intensity increases with decreasing temperature and reaches a maximum at  $T \sim 380$  K [3, 4]. The slow fluctuations associated with this scattering correspond to atomic motions correlated over a few unit cells only. In addition there is strictly elastic diffuse intensity in PMN that appears at  $T \sim 420$  K and indicates that static domains develop below that temperature [5]. The intensity of the diffuse scattering increases with decreasing temperature and saturates below  $T \sim 100$  K. These findings are in accord with a model of slowly fluctuating polar nano-regions in relaxor ferroelectrics that freeze with decreasing temperatures but do not undergo a phase transition to a long-range ferroelectric state due to the random-fields [6].

Because the size of the polar nano-regions does not exceed a few hundreds Ångströms, these give rise to the presence of diffuse scattering in both x-ray and neutron spectra. The distribution of the diffuse scattering in reciprocal space was investigated by many groups. Vakhrushev *et al.* [7] found that the diffuse scattering in PMN is predominantly transverse to the scattering vector  $\mathbf{Q}$  and that the intensity is weak near Bragg peaks with even parity  $(2h, 2k, 2l)$ . Xu *et al.* [8] investigated the distribution of diffuse scattering from

PbZn<sub>1/3</sub>Nb<sub>2/3</sub>O<sub>3</sub>-PbTiO<sub>3</sub> using x-ray techniques and found that in the (h,k,0) plane the diffuse intensity consists either of elongated streaks perpendicular to the scattering vector  $\mathbf{Q}$  (e.g. around (1,1,0)) or has the shape of a "butterfly" (e.g. around (1,0,0)). Although there is still no complete understanding of the shape and size of the PNR in relaxor ferroelectrics, it has been recognized that it is mainly correlated Pb-ions displacements that produce the diffuse scattering and are at the origin of the polar nano-regions [9]. While the direction of the Pb-displacements is difficult to obtain unambiguously from powder diffraction measurements, the average amplitude of the atomic displacements generally agrees with the results of modeling the diffuse-scattering. For example early powder neutron diffraction measurements from PMN by Bonneau *et al.* [10] showed that Pb ions are displaced from the (0,0,0) position below  $T \sim 800$  K and that the magnitude of these displacements increases with decreasing temperature. At  $T=5$  K the Pb ions are statistically displaced by  $\sim 0.36$  Å along the  $\langle 111 \rangle$  directions. The probability density function of Pb in PMN was determined [11, 12] and it is found that while at room temperature Pb is isotropically displaced, the Pb potential has a double-well shape at low temperature.

PbMg<sub>1/3</sub>Ta<sub>2/3</sub>O<sub>3</sub> (PMT) is a typical relaxor ferroelectric. As for PMN the average crystal structure is cubic at all temperatures. The real part of the dielectric permittivity has a maximum at  $T \sim 170$  K and at a frequency of  $\nu=10$  KHz. Powder neutron diffraction [14] has shown that the amplitude of the Pb displacements grows rapidly below the Burns temperature that is  $\sim 570$  K for PMT [13]. The Pb-displacements give rise to neutron diffuse scattering whose temperature dependence correlates with the temperature dependence of the atomic displacements well. Because of the similarities existing between the physical properties of PMT with those of PMN and PbZn<sub>1/3</sub>Nb<sub>2/3</sub>O<sub>3</sub> (PZN), we decided to investigate the detailed atomic structure by neutron and synchrotron radiation. The diffuse scattering of PMT in the [H,0,0]/[0,K,0] plane is transverse to the scattering vector for the (h,h,0) Bragg reflections and has a butterfly-shape near the (h,0,0) peaks. In the [H,H,0]/[0,0,L] plane the diffuse scattering of PbMg<sub>1/3</sub>Ta<sub>2/3</sub>O<sub>3</sub> is elongated along  $\langle 1,1,2 \rangle$  directions which indicates that the motion of the Pb ions have a short correlation length along that direction.

In the following we will denote  $\mathbf{Q}$  the general momentum transfer vector ( $Q = |\mathbf{Q}| = 4\pi \sin(\theta)/\lambda$ , with  $2\theta$  the scattering angle and  $\lambda$  the incident wavelength). The reciprocal lattice vectors will be denoted by  $\boldsymbol{\tau}$ , and the relative momentum transfer vector by  $\mathbf{q} = \mathbf{Q} - \boldsymbol{\tau}$ .

## II. EXPERIMENTAL RESULTS

### A. Single crystal neutron diffraction

We performed a high-quality neutron single crystal experiment from a PMT sample on D9 at ILL. The diffractometer is located on the hot source and allows access to Bragg reflections at large  $Q$  values. The short neutron wavelength of  $0.513 \text{ \AA}$ , combined with the small crystal size ( $1.6 \times 1.1 \times 0.8 \text{ mm}$ ) helped also to minimize extinction problems. Bragg intensities were collected at  $T = 20 \text{ K}$  and  $T = 300 \text{ K}$ , respectively. At room temperature 632 reflections were measured up to  $Q = 4\pi \sin(\theta)/\lambda = 15.82 \text{ \AA}^{-1}$  and 612 ( $Q \leq 19.45 \text{ \AA}^{-1}$ ) at  $T=20 \text{ K}$ , with maximum Miller index 11. A symmetry test showed that the crystal symmetry is cubic at both temperatures,  $R_{eq}=3.35\%$  for the 300 K data set and  $R_{eq}=5.92\%$  at 20 K.

The cubic symmetry describes the average periodic structure only. Atomic displacements break this symmetry locally, however the global symmetry is retained through the formation of domains. So, PMT must be described as a perturbed periodic structure. Whereas the aim of this paper is to clarify the nature of the perturbation, the diffraction data contain information about the size of the displacements that will be used as a constraint for the analysis of the diffuse scattering patterns. To analyze the atomic displacements we used the Patterson function  $P(\mathbf{u})$  that is calculated through the Fourier transform of the observed Bragg intensities:

$$P(\mathbf{u}) = \sum_{\boldsymbol{\tau}} I_{\boldsymbol{\tau}} \cos(\boldsymbol{\tau} \cdot \mathbf{u}) = \frac{1}{v} \int d^3\mathbf{r} \rho(\mathbf{r}) \rho(\mathbf{u} + \mathbf{r}) \quad (1)$$

where  $\boldsymbol{\tau}$  are the Bragg reflections,  $I_{\boldsymbol{\tau}}$  the relevant observed intensities,  $\rho(\mathbf{r})$  the scattering density and  $v$  is the unit cell volume. In order to properly set the zero of  $P(\mathbf{u})$  the value of  $I_{000}$  - calculated on the same scale after the structure refinement below described - has been added to the list of the observed intensities. Eq. 1 shows that the Patterson function is the self-convolution of the scattering density, so the position of the peaks in  $P(\mathbf{u})$  gives direct access to the interatomic distances  $\mathbf{u}$  [26]. Cuts through the Patterson maps across the main interatomic peaks are shown in Fig. 1. The most pronounced characteristic in the cut through the Patterson map shown in Fig. 1 is visible in the Pb-B interatomic peaks. At room temperature the Pb-B average length is  $\sim 2.5 \text{ \AA}$  with a distribution of  $\sim 0.3 \text{ \AA}$ . At low temperature the Pb-B length shows a maximum away from the expected distance in the perovskite structure. As B-O peaks do not show anything similar, we must attribute

this feature to displacements of Pb atoms from their average position. At room temperature the Pb atoms lie in a spherical region about their nominal positions. At  $T = 20$  K, the Pb displacements are more defined and Pb atoms lie on an isotropic spherical shell. This can be described by a 3-D double-well-shaped potential defining the Pb displacements.

Moreover, a least-square fit to the diffraction data was done using the programs `jana2000` [27]. The refined atomic parameters are summarized in Table I. In agreement with the analysis of Vakhrushev *et al.* [12] for PMN, the structural refinement at  $T = 20$  K indicates simultaneous displacements of the Pb ions along all directions by  $0.34(2)\text{\AA}$ . The displacements of the O ions are modeled by anisotropic temperature factors. The result of the refinement gives that the O thermal ellipsoids have a larger component in the  $\langle 110 \rangle$ -plane. We also observe that the oxygen-related Patterson peaks increase and get sharper with increasing temperature, which is direct evidence for the anomalous decrease of the thermal displacement parameters of the oxygen atoms observed in a previous powder diffraction experiment [14]. So, while we cannot disregard the possibility of O displacements correlated with the Pb displacements, this is not a dominant feature. We could not obtain from the diffraction evidence about the anisotropy of the displacements, although the spatial resolution would be in principle sufficient for this purpose. We attribute this limitation to either the averaging over many symmetry-equivalent PNR domains or to a large fraction of thick domain walls (or non-polar regions [1]) between PNR, that are not ordered. Furthermore even in ordered PNR the displacements are only broadly collinear. However, the results obtained from the diffraction data allow us to restrict the analysis of the diffuse scattering to Pb displacements only.

## B. X-ray diffuse scattering

The diffuse scattering was measured in a single crystal of PMT at the Swiss-Norwegian Beam Line (SNBL) at the ESRF. The measurements were performed in transmission geometry with the wavelength  $\lambda = 0.71076\text{\AA}$  in a broad temperature range between  $T = 100$  K and 450 K. Systematic maps of scattered intensity were collected by a MAR-345 imaging plate detector with the single crystal being rotated in steps of  $0.5^\circ$  around the vertical axis. From this data the distribution of the diffuse intensity in the  $[H,0,0]/[0,K,0]$  and  $[H,H,0]/[0,0,L]$  scattering planes could be reconstructed, using the program `CrysAlis` by Oxford Diffraction

to merge the measured maps.

Figure 2 shows the reconstruction of the scattered intensity distribution in the  $[H,0,0]/[0,K,0]$  and  $[H,H,0]/[0,0,L]$  scattering planes at  $T = 175$  K. As known from previous neutron measurements, diffuse scattering is particularly strong at this temperature. The diffuse scattering in PMT has a similar "butterfly"-shaped distribution as found in PMN around the  $(2,0,0)$  Bragg reflection and within the  $[H,0,0]/[0,K,0]$  scattering plane as shown in Fig. 2a. It can be observed that the diffuse scattering is elongated along the four equivalent  $\langle 1,1,0 \rangle$  directions around these zone centers, while the diffuse scattering is essentially transverse to the scattering vector  $\mathbf{Q}$  around the  $(2,2,0)$  Bragg peak. Comparing these measurements with the diffuse scattering obtained when the single crystal is aligned in the  $[H,H,0]/[0,0,L]$  plane shows firstly that the diffuse scattering is extended along the  $\langle 1,1,2 \rangle$  directions around the  $(2,0,0)$  Bragg peak. Secondly, it can be observed in Fig. 2b the diffuse scattering around the  $(2,2,0)$  Bragg peak has four wings of intensity that extend along the  $\langle 1,1,2 \rangle$  directions and no diffuse intensity is visible along the  $\langle 1,1,0 \rangle$  directions. This last observation shows that the intensity of the diffuse scattering depends on the direction of the atomic displacements relative to the orientation of the scattering vector  $\mathbf{Q}$ . The same effect was observed in PMN [8, 15], where the diffuse scattering was modeled by introducing a polarization factor of the form  $(\mathbf{Q} \cdot \mathbf{u})^2$ . Although this polarization factor has the same form as for phonon scattering, it is also present in the cross-section for diffuse x-ray and neutron scattering if atoms are displaced from the average position in the unit cell. In the latter case, the diffuse intensity varies like  $(\mathbf{Q} \cdot \mathbf{u})^2$  with  $\mathbf{u}$  the direction of the atomic displacements [16]. It is this polarization factor that causes the absence of the diffuse intensity when the displacement disorder is perpendicular to the scattering vector  $\mathbf{Q}$  as we observe for PMT in the vicinity of the  $(1,1,0)$  Bragg peak. As the diffuse scattering in PMT at low temperatures was found to be truly elastic from neutron diffraction measurements [17], it must originate from static random displacements, rather than from the condensation of a transverse optic phonon mode.

### III. MODEL OF THE DIFFUSE SCATTERING IN PMT

To analyze the diffuse scattering in PMT we introduce a model that takes into account the shape of the polar nanoregions as well as the direction and amplitude of the displacements.

We define therefore a shape function  $S(\mathbf{r})$  for a PNR. The autocorrelation function  $G(\mathbf{r})$  of  $S(\mathbf{r})$  is

$$G(\mathbf{r}) = \int d^3\mathbf{r}' S(\mathbf{r}') S(\mathbf{r} - \mathbf{r}'), \quad (2)$$

and its Fourier transform

$$\tilde{G}(\mathbf{Q}) = \int d^3\mathbf{r} G(\mathbf{r}) \exp(-i\mathbf{Q} \cdot \mathbf{r}). \quad (3)$$

For the case of a periodic crystal of limited dimensions described by  $S(\mathbf{r})$ , the diffracted intensity is given by

$$I(\mathbf{Q}) = |F(\mathbf{Q})|^2 \sum_{\boldsymbol{\tau}} \tilde{G}(\mathbf{Q} - \boldsymbol{\tau}), \quad (4)$$

where  $F(\mathbf{Q}) = \sum_j \rho_j(\mathbf{r}) \exp(-i\mathbf{Q} \cdot \mathbf{r}_j)$  is the structure amplitude of one unit cell and  $\rho_j(\mathbf{r})$  the scattering density of atom  $j$ ;  $\boldsymbol{\tau}$  is a reciprocal lattice vector.

For a disordered crystal the scattering density  $\rho(\mathbf{r})$  [28] can be decomposed into an average atomic density  $\rho_a(\mathbf{r}) \propto \delta(\mathbf{r} - \mathbf{r}_j)$  and a random density  $\rho_b(\mathbf{r}) \propto \delta(\mathbf{r} - \mathbf{r}_j - \mathbf{u}) - \delta(\mathbf{r} - \mathbf{r}_j)$ , so that the atomic distribution in the crystal is described by  $\rho(\mathbf{r}) = \rho_a(\mathbf{r}) + \rho_b(\mathbf{r})$ . The average atomic structure contributes to the Bragg reflections and its scattered intensity is vanishingly small away from the reciprocal lattice vectors. In that case it is justified to neglect interference effects and to make the assumption that  $|F(\mathbf{Q})|^2 \approx |F_a(\mathbf{Q})|^2 + |F_b(\mathbf{Q})|^2$ . In this approximation the total scattered intensity consists of the superposition of Bragg peaks with broad diffuse components centered around the lattice reciprocal vectors.

### A. The form factor

The diffuse scattering measured in PMT was modeled by assuming that only the Pb ion is displaced from its average position ( $\mathbf{r}_{\text{Pb}} = (0, 0, 0)$  in the  $Pm\bar{3}m$  space group). If we suppose that the Pb atom is displaced by a vector  $\mathbf{u}$ , we obtain for the random density

$$F_b(\mathbf{Q}) = b_{\text{Pb}} [e^{-i\mathbf{Q} \cdot (\mathbf{r}_{\text{Pb}} + \mathbf{u})} - e^{-i\mathbf{Q} \cdot \mathbf{r}_{\text{Pb}}}], \quad (5)$$

where  $b_{\text{Pb}}$  is the form factor (including Debye-Waller) of Pb ion in the unit cell. As in our simplified model the cubic unit cell of PMT contains only one ion (Pb) that is displaced from its average site, the form factor of the diffuse intensity reduces to

$$|F_b(\mathbf{Q})|^2 = 2b_{\text{Pb}}^2 [1 - \cos(\mathbf{Q} \cdot \mathbf{u})] = 4b_{\text{Pb}}^2 \sin^2(\mathbf{Q} \cdot \mathbf{u}/2). \quad (6)$$

For small values of  $\mathbf{Q} \cdot \mathbf{u}$  eq. 6 is  $\propto (\mathbf{Q} \cdot \mathbf{u})^2$  which is the form used in refs. 8, 15.

It is instructive to give here the  $\mathbf{Q}$ -dependence of the diffuse scattering when Pb ions in the *average* structure are located on a spherical shell of radius  $u$ , *i.e.*

$$\rho_a(\mathbf{r}) = b_{Pb} \frac{\delta(|\mathbf{r} - \mathbf{r}_{Pb}| - u)}{4\pi u^2}, \quad (7)$$

as suggested by neutron diffraction in both PMN refs 10, 12 and PMT (*cf.* Sec. II B and ref. 14). In that case, we obtain

$$F_b(\mathbf{Q}) = b_{Pb} e^{-i\mathbf{Q} \cdot \mathbf{r}_{Pb}} \left[ e^{-i\mathbf{Q} \cdot \mathbf{u}} - \frac{\sin(Qu)}{Qu} \right], \quad (8)$$

and the scattered diffuse intensity is modulated by a structure factor

$$|F_b(\mathbf{Q})|^2 = b_{Pb}^2 \left[ 1 + \left( \frac{\sin(Qu)}{Qu} \right)^2 - 2 \frac{\sin(Qu)}{Qu} \cos(\mathbf{Q} \cdot \mathbf{u}) \right], \quad (9)$$

whose first nonzero term in the small-  $\mathbf{Q} \cdot \mathbf{u}$  expansion is still  $\propto (\mathbf{Q} \cdot \mathbf{u})^2$ .

Finally it should be pointed out that the dependence of the diffuse intensity in the case of atomic displacements differs from Huang scattering that arises for small concentrations of defects. In this case, the displacements distribution has spherical symmetry around a defect and the scattering is proportional to  $I_{Huang} \propto (Q \cos(\phi))^2 / q^2$ , where  $\phi$  is the angle between  $\mathbf{Q}$  and the wave-vector  $\mathbf{q}$ . Huang scattering is present around all Bragg reflections and its intensity is enhanced along the scattering vector  $\mathbf{Q}$  while the diffuse intensity vanishes when  $\mathbf{Q} \perp \mathbf{q}$ . Inspection of the diffuse scattering measured in PMT at  $T = 175$  K shows that the planes of zero intensity are not always perpendicular to  $\mathbf{Q}$ . For example Fig. 2 shows that the diffuse scattering measured in PMT around the (1,1,0) Bragg position with the crystal being oriented with an  $[0,0,1]$  axis vertical is elongated in the direction transverse to the scattering vector and is zero along  $\mathbf{Q}$ . Both results are contrary to what would be expected for Huang scattering. We note that it was found that weak diffuse scattering is still present in PMN above the Burns temperature, with, however, a different distribution of intensity in reciprocal space. At high temperature this residual diffuse scattering could mainly arise from Huang scattering and the chemical disorder on the B-site. On the other hand correlated atomic displacements, which give rise to the strong diffuse scattering, disappear above the Burns temperature [18].



## B. The choice of the line-shape

The line-shape of the diffuse scattering depends upon the shape function  $S(\mathbf{r})$  that describes the form and the size of the polar nanoregions. In the simplest assumption, if Pb displacements were to be perfectly aligned within any sharply defined geometric region, there would be characteristic intensity modulations, which have not been observed. Moreover, Monte-Carlo simulations of the diffuse scattering in PMN have shown that the domain wall structure of the polar nanoregions is complicated [21] which makes it difficult to describe the shape-function with a simple analytical function. However, the autocorrelation of the shape  $G(\mathbf{r})$  can be described by an analytical function. In fact, shape in this case is defined in a stochastic way.

Hereafter we choose to describe  $G(\mathbf{r})$  by decaying exponentials with an anisotropic decay length. Depending on the detailed symmetry of the decay length, this leads to power-law decay of the diffuse scattering. In fact, it has been demonstrated in PMN that the line-shape of the diffuse scattering generally follows a  $q^{-\alpha}$ -dependence, with  $\alpha > 2$  and weakly depending on  $T$ , becoming higher at room temperature [19]. Others (Chetverikov *et al.* [24] found that  $\alpha$  varies between 1.5 and 2.6 as a function of the temperature. The "pancake" model of Xu *et al.* [8] assumes that PNR have cylindrical symmetry, which yields an exponent  $\alpha = 2$  along the axis,  $\alpha = 3$  in the orthogonal plane, and higher along general directions [20]. In the following we will assume a more general (orthorhombic) anisotropy of the autocorrelation function, keeping its exponential character:

$$\begin{aligned} G(\mathbf{r}) &= e^{-\mathbf{w}_1 \cdot \mathbf{r}/L_1} e^{-\mathbf{w}_2 \cdot \mathbf{r}/L_2} e^{-\mathbf{w}_3 \cdot \mathbf{r}/L_3}; \\ \tilde{G}(\mathbf{q}) &= C \frac{1}{1 + (L_1 \mathbf{w}_1 \cdot \mathbf{q})^2} \frac{1}{1 + (L_2 \mathbf{w}_2 \cdot \mathbf{q})^2} \times \\ &\quad \times \frac{1}{1 + (L_3 \mathbf{w}_3 \cdot \mathbf{q})^2}. \end{aligned} \tag{10}$$

$L_1, L_2, L_3$  correspond then to the average dimensions of the polar nanoregions along the mutually orthogonal directions defined by the unit vectors  $\mathbf{w}_i$  ( $i=1,2,3$ ),  $C$  is an inessential constant. This is consistent with power-law decay with  $2 < \alpha < 4$  along special directions ( $\alpha \leq 6$  in general).

#### IV. INTERPRETATION OF THE DIFFUSE SCATTERING IN PMT

In order to model the diffuse scattering in PMT, the direction of the static displacements has to be known. There is however no consensus about the direction of the Pb displacement in the literature. In Xu's analysis [8] of the diffuse scattering in PMN, the polarization (displacement) direction is parallel to  $\langle 1, -1, 0 \rangle$ . In contrast using neutron scattering and a pair distribution function analysis, Jeong *et al.* [22] found direct evidence that displacements in PMN have rhombohedral symmetry, which suggests that the Pb atoms are displaced along the  $\langle 1, 1, 1 \rangle$  direction. Initially we assume that ionic displacements  $\mathbf{u}$  are along the  $\langle 1, -1, 0 \rangle$  equivalent directions, and choose the unit vectors that define the dimensions of the PNR as  $\mathbf{w}_1=[1,1,0]/\sqrt{2}$ ,  $\mathbf{w}_2=[1,-1,0]/\sqrt{2}$  and  $\mathbf{w}_3=[0,0,1]$ , respectively. In this model, there are six domains which correspond to the symmetrically equivalent  $\langle 1, 1, 0 \rangle$  directions in the cubic structure. When  $L_1 \ll L_2 = L_3$ , the model is equivalent to the "pancake" model of the PNR of ref. 8. This model accounts properly for the distribution of the diffuse scattering in PMT in the  $(1,0,0)$  Brillouin zones with  $\langle 0, 0, 1 \rangle$  perpendicular to the scattering plane when  $L_1 \sim 20 \text{ \AA}$  and  $L_2 = L_3 \sim 100 \text{ \AA}$ . In the  $[\text{H},\text{H},0]/[0,0,L]$  scattering plane, the diffuse scattering has the shape of a "butterfly" with wings along the  $\langle 1, 1, 1 \rangle$  directions that is reproduced by the calculations. We find, however, that this model does not reproduce the distribution of diffuse scattering intensities around the  $(2,2,2)$  Bragg peak properly. In fact, the measurements clearly show that diffuse scattering is mainly transverse to the scattering vector  $\mathbf{Q}$ , as shown in Fig. 2b, while this model yields additional streaks along  $\mathbf{Q}$  that cannot be eliminated alone by adjusting the correlation lengths. We then concluded that the transverse streak is cancelled because of the form factor  $\propto (\mathbf{Q} \cdot \mathbf{u})^2$ . In addition, inspection of the diffuse intensity map in PMT reveals that in the  $[\text{H},\text{H},0]/[0,0,L]$  scattering plane the streaks of diffuse scattering around the  $(0,0,1)$  Bragg peaks are extended along the  $\pm \langle 1, 1, \mp 2 \rangle$  directions which indicates that the length of the polar nanoregions must be short along these directions. The simplest way of building PNR with e.g. a short  $\langle 1, 1, -2 \rangle$  extension is to choose  $\mathbf{w}_1 = 1/\sqrt{2}[1, -1, 0]$ ,  $\mathbf{w}_2=1/\sqrt{3}[1, 1, 1]$  and  $\mathbf{w}_3=1/\sqrt{6}[1,1,-2]$ . In this case there are 12 possible PNR domains that will contribute to the patterns of diffuse intensity. The diffuse scattering distribution was calculated for displacements  $\mathbf{u}$  along these directions and the best agreement between observed and calculated diffuse intensity patterns could be obtained by choosing  $\mathbf{u}$  along  $\langle 1, 1, 1 \rangle$ . For the other

directions of atomic displacements the distribution of intensity wings around some of the Bragg peaks were incorrect.

In the previous section we showed that the model with the Pb determined the direction of the most probable Pb-displacements in PMT as  $\langle 1, 1, 1 \rangle$ , the dimensions of the parallelepiped could be estimated from the width of the diffuse intensity away from the Bragg peaks. At  $T = 175$  K, a reasonable estimation yields  $L_1 \sim 50$  Å;  $L_2 \sim 30$  Å and  $L_3 \sim 4$  Å. Calculated diffuse scattering maps are shown in Figs. 3a and 3b and can be compared with the experimental data presented in Fig. 2.

## V. DISCUSSION AND CONCLUSIONS

Our main results can be summarized as follows:

- i) Patterson analysis provides direct evidence that the potential at Pb sites develops a double-well structure at low temperature causing Pb ions to be distributed on a shell with radius  $\approx 0.3$  Å. The observed extinction of some diffuse streaks is in agreement with the form of the structure factor given by eqs 6,9. In addition it should be possible to measure the change in the Pb potential with temperature by computing the diffuse scattering intensities as a function of scattering vector  $\mathbf{Q}$ . As the displacements are important ( $u \approx 0.2...0.3$ Å), this would require recording the distribution of the diffuse scattering intensity at large scattering vectors. Having Pb ions displaced along the  $\langle 1, 1, 1 \rangle$  direction is consistent with the analysis of the local structure of relaxor ferroelectrics by PDF [22] and with the observations of a rhombohedral phase transition that can be induced by application of an electric field [23]. Also recent dielectric measurements in PMN doped with PbTiO<sub>3</sub> in applied electric field have shown that the spontaneous polarization in the polar nanoregions is along  $\langle 1, 1, 1 \rangle$  [25].
- ii) Describing the structure of the polar nanoregions in terms of Pb-displacements only might be a too simple model. From single crystal data, we have only indirect evidence for displacements of cations at B and O sites. These ions then probably play a less important role in the formation of diffuse scattering. However, we note that qualitative understanding of x-ray diffuse scattering could be obtained by considering only Pb displacements. This might be due to the smaller x-ray cross-section of O compared

with the metal cations. Neutron diffuse scattering analysis could then probably shed more light on O behavior if the diffuse scattering was measured with a higher quality than what was possible up to now.

- iii) The main structural feature causing the characteristic butterfly diffuse scattering in PMT is the formation of PNR where Pb atoms are displaced along one  $\langle 1, 1, 1 \rangle$  direction; PNR have large correlation lengths, except along the  $\langle 1, 1, -2 \rangle$  direction orthogonal to the Pb displacement direction, thereby confirming the 'pancake' model of ref. [8], but with a different geometry.

In conclusion, we have analyzed the distribution of displacements in PMT by single crystal neutron diffraction and synchrotron radiation. The diffuse scattering and especially its structural origin have been understood qualitatively. Another interesting topic is the relationship between coherent Pb  $\langle 111 \rangle$ -displacements in PNRs and the known B-site partial ordering, with  $(1/2, 1/2, 1/2)$  broad satellites (see Fig. 2b) pointing to an ordering of  $[111]$  B-site planes with alternating full-B'' (Ta) layers and  $2/3\text{-B}', 1/3\text{-B}''$  layers. A comprehensive and detailed microstructural study of all systematic atomic displacements is necessary to understand this relationship and to bridge the gap between structure and macroscopic properties of relaxor ferroelectrics.

## VI. ACKNOWLEDGMENT

Work based on experiments performed at the Swiss-Norwegian Beamline SNBL and the Institute Laue-Langevin ILL of Grenoble, France. We thank D. Chernyshov (SNBL) for his assistance with measurements of the diffuse scattering. RAC wishes to thank the Leverhulme trust for their financial support. This work was partially supported by the Swiss National Foundation (Project No. 20002-111545).

- 
- [1] G.A. Smolenskii and A.I. Agranovskaya, Soviet Physics Solid State **1**, 1429 (1959).
  - [2] G. Burns and B.A. Scott, Solid State Commun. **13**, 423 (1973) .
  - [3] S.N. Gvasaliya, S.G. Lushnikov and B. Roessli, Phys. Rev. B **69**, 092105 (2004).
  - [4] H. Hiraka, S.H. Lee, P.M. Gehring, G.Y. Xu and G. Shirane, Phys. Rev. B **70**, 184105 (2004).

- [5] S.N. Gvasaliya, B. Roessli, R.A. Cowley, P. Huber and S.G. Lushnikov, J. Phys.: Condensed Matter **17**, 4343 (2005).
- [6] R.A. Cowley, S.N. Gvasaliya and B. Roessli, Ferroelectrics **378**, 53 (2009).
- [7] S.B. Vakhrushev, A.A. Naberezhnov, N.M. Okuneva, and B.N. Savenko, Phys. Solid State **37**, 1993 (1995).
- [8] G. Xu, Z. Zhong, H. Hiraka, and G. Shirane, Phys. Rev. B **70**, 174109 (2004).
- [9] T.R. Welberry, D.J. Goossens and M.J. Gutmann, Phys. Rev. B **74**, 224108 (2006).
- [10] P. Bonneau, P. Garnier, G. Calvarin, E. Husson, J.R. Gavarri, A.W. Hewat and A. Morell, J. Solid State Chem. **91**, 350 (1991).
- [11] V.V. Chernyshev, S.G. Zhukov, A.V. Yatsenko, L.A. Aslanov and H. Schenk, Acta Cryst. **A50**, 601 (1994).
- [12] S.B. Vakhrushev and N.M. Okuneva, in Fundamental Physics of Ferroelectrics 2002, edited by Ronald E. Cohen, AIP Conf. Proc. **626** (AIP, Melville, NY, 2002), p. 117.
- [13] O.Yu. Korshunov, P.A. Markovin, and R.V. Pisarev, Ferroelectrics **13**, 137 (1992 ).
- [14] S.N. Gvasaliya, B. Roessli, D. Sheptyakov, S.G. Lushnikov and T.A. Shaplygina, Eur. Phys. J. B **40**, 235 (2004).
- [15] H. You and Q.M. Zhang, Phys. Rev. Lett. **79**, 3950 (1997).
- [16] M.A. Krivoglaz, *Theory of X-ray and Thermal-Neutron Scattering by Real Crystals*, (Plenum, New-York, 1969).
- [17] S.N. Gvasaliya, S.G. Lushnikov and B. Roessli, Europhys. Lett. **63**, 303 (2003).
- [18] see Fig.2 in P. M. Gehring, H. Hiraka, C. Stock, S.-H. Lee, W. Chen, Z.-G. Ye, S. B. Vakhrushev and Z. Chowdhuri, arXiv:0904.4234v1 [cond-matt.]
- [19] H. You, J. Phys. Chem. Solids **61**, 215 (2000).
- [20] If the autocorrelation function has cylindrical symmetry  $G(\mathbf{r}) = \exp(-|\frac{\mathbf{w}_1 \cdot \mathbf{r}}{L_1}|) \exp(-\frac{r_{\perp}}{L_r})$  with  $L_1$  along the cylinder axis and  $L_r$  perpendicular to it, the Fourier transforms is  $\tilde{G}(\mathbf{Q}) = 2\pi L_r^2 L_1 / (1 + (2\pi L_1(\mathbf{w}_1 \cdot \mathbf{q})^2) / (1 + (2\pi L_r q_{\perp})^2)^{1.5}$ .
- [21] M. Paściak, M. Wołczyr and A. Pietraszko, Phys. Rev. B **76**, 014117 (2007).
- [22] I.-K. Jeong , T. W. Darling, J. K. Lee, Th. Proffen, R. H. Heffner, J. S. Park, K. S. Hong, W. Dmowski and T. Egami, Phys. Rev. Lett. **94**, 147602 (2005).
- [23] G. Calvarin, E. Husson and Z.G. Ye, Ferroelectrics **165**, 349 (1995).
- [24] Y.O. Chetverikov, A.A. Naberezhnov, S.B. Vakhrushev, B. Dorner, and A.S. Ivanov, Appl.

- Phys. A: Mater. Sci. Process. **A74**, S989 (2002).
- [25] Zhenrong Li, Zhuo Xu, Xi Yao and Z.-Y. Cheng, J. Appl. Phys. **104**, 024112 (2008).
- [26] C. Giacovazzo, H.L. Monaco, D. Viterbo, F. Scordari, G. Gilli, G. Zanotti, and M. Catti, "Fundamentals of Crystallography" (1992, Oxford: Oxford University Press).
- [27] V. Petricek, M. Dusek, and L. Palatinus (2000). Jana2000. The crystallographic computing system. Institute of Physics, Praha, Czech Republic.
- [28] We neglect here Debye-Waller and atomic form factors.

TABLE I: Atomic parameters obtained for PMT at  $T = 20$  K. The atomic displacements are modeled with three split positions for the Pb ions ( $\text{Pb}_x$ : Pb displacements along  $\langle 1, 0, 0 \rangle$ ;  $\text{Pb}_{xx}$  along  $\langle 1, 1, 0 \rangle$  and  $\text{Pb}_{xxx}$  along  $\langle 1, 1, 1 \rangle$ ). G is the number of ions in the unit cell;  $B_{22}=B_{11}$ ,  $B_{33}$  anisotropic and  $B_{iso}$  isotropic temperature factors in ( $\text{\AA}^2$ ).

Atom	G	x	y	z	$B_{11}$	$B_{33}$	$B_{iso}$
20 K							
$\text{Pb}_x$	1/3	0.090(4)	0	0	-	-	0.88(7)
$\text{Pb}_{xx}$	1/3	0.056(4)	x	0	-	-	0.88(7)
$\text{Pb}_{xxx}$	1/3	0.045(3)	x	x	-	-	0.88(7)
O	3	1/2	1/2	0	1.86(4)	0.960(4)	
Ta/Mg	1	1/2	1/2	1/2	0.586(8)	$B_{11}$	
300 K							
$\text{Pb}_x$	1/3	0.076(9)	0	0	-	-	1.2(2)
$\text{Pb}_{xx}$	1/3	0.05(1)	x	0	-	-	1.2(2)
$\text{Pb}_{xxx}$	1/3	0.046(8)	x	x	-	-	1.2(2)
O	3	1/2	1/2	0	1.96(7)	0.85(7)	
Ta/Mg	1	1/2	1/2	1/2	0.62(2)	$B_{11}$	

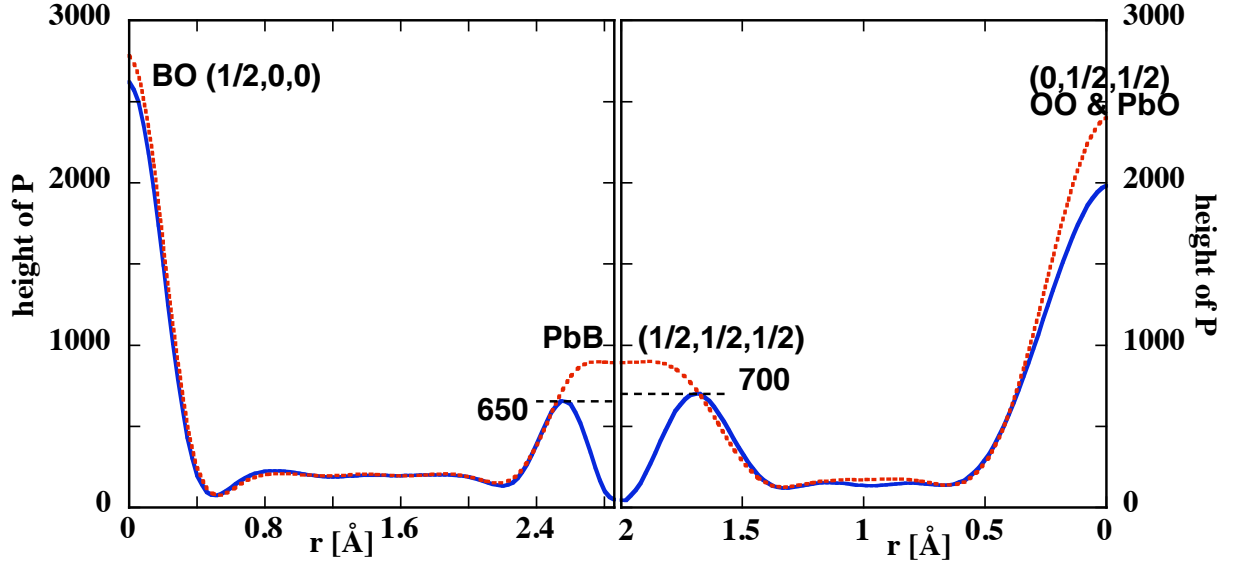


FIG. 1: Linear cuts through the Patterson maps at 20 K (blue) and 300 K (red) along the  $\langle 0, 1, 1 \rangle$  (*left*) and  $\langle 1, 0, 0 \rangle$  (*right*) directions. Endpoints in crystal coordinates are shown for clarity, together with the atom pairs corresponding to the relevant Patterson map peaks.



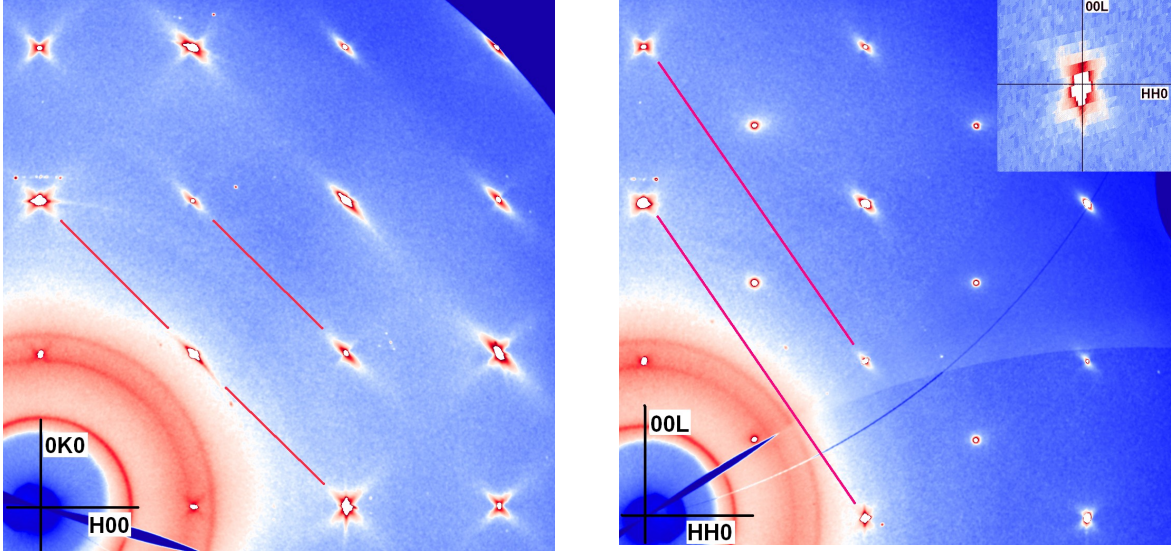


FIG. 2: a) False-color reconstructed image of experimental diffuse scattering intensities from PMT in the  $[H,0,0]/[0,K,0]$  scattering plane. The direction of streaks of diffuse intensity are shown by a solid line and extend along the  $\langle 1,1,0 \rangle$ -type directions. b) False-color image of experimental intensities from PMT in the  $[H,H,0]/[0,0,L]$  scattering plane. The direction of streaks of diffuse intensity are shown by a solid line and extend along the  $\langle 1,1,2 \rangle$ -type directions. The intensity spots visible at the  $\frac{1}{2}(h,h,l)$  positions are due to partial order in the B-sublattice. The data was taken at  $T=175$  K. The inset to Fig. 2b shows the distribution of the diffuse scattering around the  $(2,2,0)$  Bragg peak. The distance from the center of the inset to the boundaries along the  $\langle H,H,0 \rangle$  and  $\langle 0,0,L \rangle$  directions is  $0.78\text{\AA}^{-1}$ . Note that the diffuse scattering is elongated along the  $\langle 1,1,2 \rangle$  direction.

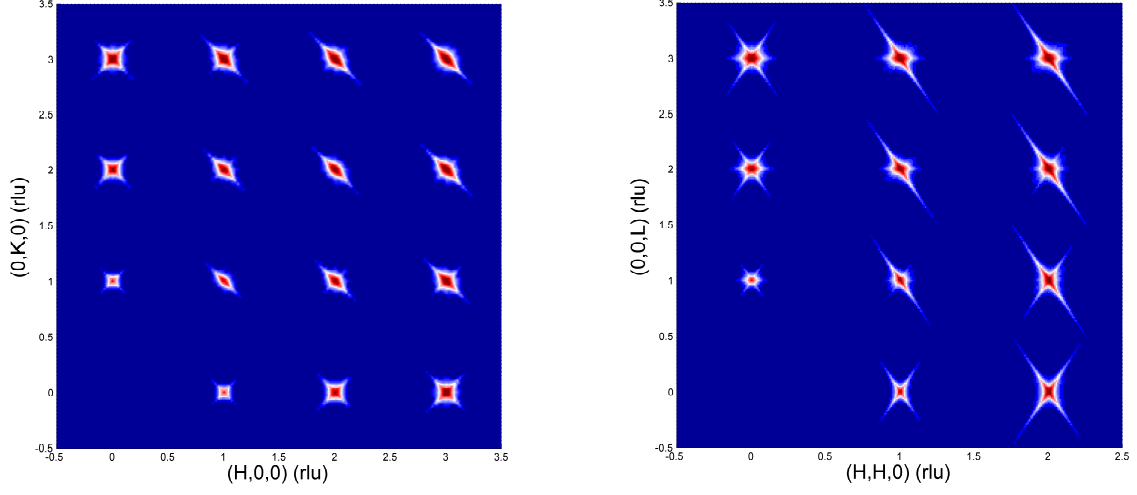


FIG. 3: False-color images of calculated diffuse scattering intensities from PMT a) in the  $[H,0,0]/[0,K,0]$ - and b) in the  $[H,H,0]/[0,0,L]$ -scattering planes. The intensities are given in a logarithmic scale.